RSC Advances

PAPER

View Article Online
View Journal | View Issue

Check for updates

Cite this: *RSC Adv.*, 2025, **15**, 18324

A floatable TiO_2–Ag photocatalyst enables effective antibiotic degradation and pathogen growth control†

Minh Thi Nguyen,[a] Phuong Thu Ha,[b] Thi Thu Huong Le,[c] Huong Giang Bui,[a] Ke Son Phan,[b] Nhat Huy Chu,[a] Thi Thu Trang Mai,[b] Thuy Dieu Thi Ung,[b] Anh Tuyet Thi Le[a] and Phuong Ha Hoang *[a]

This study explores the powerful capabilities of a floatable photocatalyst, TiO_2–Ag immobilized on expanded clay (EC), for photocatalytic antibiotic degradation and pathogen inhibition in aquaculture systems. The porous and floatable nature of EC makes it an ideal carrier for enhancing photocatalytic activity, enabling the easy recovery and reusability of TiO_2–Ag. The synthesis of TiO_2–Ag/EC is optimized by adjusting TiO_2–Ag concentration, integration time, and stirring speed, with a peak Ti content of 2584.51 ± 49.52 ppm achieved under specific conditions (35 000 ppm TiO_2–Ag, 12 hours integration, 100 rpm stirring). Remarkably, within 2 hours of sunlight exposure, TiO_2–Ag/EC (10% w/v) reduced the pathogenic density of *Vibrio harveyi*, *Vibrio parahaemolyticus*, and *Escherichia coli* from 10^6 CFU mL^{-1} to under 100 CFU mL^{-1}, maintaining antibacterial efficacy even after seven cycles. Beyond pathogen control, TiO_2–Ag/EC degraded over 92% of tetracycline and oxytetracycline at pH 7–9 and achieved up to 95.7% rifampicin removal at pH 5, within 4 hours of sunlight exposure. The degraded antibiotic solution lost its bactericidal activity, suggesting the safety of the formed byproducts for the environment. Notably, at the TiO_2–Ag/EC addition ratio of 2.5% w/v, equivalent to a Ti concentration of approximately 62.5 ppm, the material reached a maximum COD removal efficiency of 82.7 ± 2.0% after 40 hours of illumination. These results highlight the potential of TiO_2–Ag/EC as a sustainable solution for eliminating antibiotic residues, organic matter, and controlling disease spread in aquaculture environments.

Received 4th April 2025
Accepted 21st May 2025

DOI: 10.1039/d5ra02333e

rsc.li/rsc-advances

Open Access Article. Published on 02 June 2025. Downloaded on 5/21/2026 6:09:23 AM.
This article is licensed under a Creative Commons Attribution-NonCommercial 3.0 Unported Licence.

Introduction

The rapid expansion of high-density shrimp farming has given rise to significant environmental challenges, particularly in the form of pathogenic bacteria and antibiotic residues. Shrimp feed typically contains 33–45% protein, however, only a fraction of nitrogen (24–37%) and phosphorus (13–28%) are utilized by the shrimp.[1] The accumulation of excess organic nutrients not only pollutes the water but also creates a favorable environment for disease outbreaks, undermining shrimp growth and survival rates. Traditionally, various types of synthetic antibiotics have been widely used to control pathogens. However, up to 75% of the antibiotics fed to aquatic animals are excreted into the water, causing a high risk of the emergence of antibiotic-resistant bacteria and human health.[2] A study by Pesi *et al.* showed that up to 90% of aquatic bacteria have developed the resistance to at least one antibiotic. Among them, antibiotic-resistant genes are commonly found in *Escherichia coli*, *Aeromonas,* and *Vibrio* genus.[3] These ongoing challenges highlight the urgent need for effective treatment solutions that can manage pathogen spread and reduce antibiotic residues in the environment, thereby preserving water quality and ensuring the sustainability of aquaculture.

Antibiotics degrade through several processes, including photodegradation, hydrolysis, and biodegradation, with their effectiveness largely influenced by environmental factors such as pH, temperature, and chemical composition.[4] Biological methods are favored due to their low cost and environmental benefits, but modern antibiotics have complex chemical structures that can hinder bacterial growth and disrupt microbial metabolism. This challenge complicates bacterial-based degradation methods and raises concerns about the development of antibiotic-resistant genes.[5] While physical filtration membranes can adsorb antibiotics, they suffer from frequent clogging, which increases maintenance costs and limits their widespread application.[6]

[a]*Institute of Biology, Vietnam Academy of Science and Technology, 18 Hoang Quoc Viet Road, Cau Giay District, Hanoi 100000, Vietnam. E-mail: hph@ibt.ac.vn*
[b]*Institute of Materials Science, Vietnam Academy of Science and Technology, 18 Hoang Quoc Viet Road, Cau Giay District, Hanoi 100000, Vietnam*
[c]*Vietnam National University of Agriculture, Trau Quy, Gia Lam District, Hanoi 100000, Vietnam*

† Electronic supplementary information (ESI) available. See DOI: https://doi.org/10.1039/d5ra02333e

© 2025 The Author(s). Published by the Royal Society of Chemistry

Open Access Article. Published on 02 June 2025. Downloaded on 5/21/2026 6:09:23 AM. This article is licensed under a Creative Commons Attribution-NonCommercial 3.0 Unported Licence.

Chemical methods using photocatalysts like TiO_2–Ag nanoparticles have gained attention for their ability to degrade pollutants effectively. Photocatalysis offers distinct advantages, including the use of light energy to generate reactive oxygen species (ROS) that can break down pollutants under normal temperature and pressure conditions, converting organic contaminants into harmless byproducts like CO_2 and H_2O.[7] ROS can also penetrate bacterial cells, damaging vital components such as proteins, DNA, and lipids, leading to cell death. These properties make photocatalysis a promising approach for addressing antibiotic pollution and controlling pathogenic bacteria in the environment.[8] However, a major challenge is the recovery of photocatalytic particles after use. These powder nanoparticles often aggregate or remain suspended in the solution, reducing their active surface area, limiting pollutant interactions, and decreasing light absorption efficiency. Furthermore, the lack of established regulations surrounding the management of photocatalytic materials raises concerns about secondary pollution from nano-sized particles.[9]

Therefore, in the last few years, attention has been paid to designing the floatable photocatalyst to enable the easy recovery and reusability of the material. In contrast to powder material, floatable photocatalysts owe their unique advantage of direct sunlight irradiation without the attenuation caused by water, hence, enhancing photocatalytic performance.[10] In previous research, the expanded clay (EC) carriers were successfully fabricated by pyrolyzing a mixture of clay and rice husk at 1200 °C, followed by rapid cooling. This process results in a rigid, porous structure that efficiently integrates and protects the TiO_2–Ag photocatalyst. The floatable nature of expanded clay enhances light exposure and maximizes oxygen involvement in the photocatalytic degradation process at the water/air interface. Preliminary results show that TiO_2–Ag immobilized on expanded clay can inhibit *Vibrio parahaemolyticus* by up to 99% within 2 hours of halogen lamp illumination.[11] Building on these findings, the present study will optimize the integration of TiO_2–Ag onto expanded clay and evaluate its ability to inhibit a range of pathogenic bacteria and degrade commonly used antibiotics in aquaculture environments. The photocatalytic performance of TiO_2–Ag/EC will be assessed under natural sunlight to provide a realistic evaluation of its efficiency in the wastewater treatment process. Ultimately, this research aims to confirm the potential practical significance of TiO_2–Ag/EC composites as a sustainable solution for tackling pollution and disease in aquaculture systems.

Experimental

Materials

The pathogenic bacteria, *Escherichia coli, Vibrio harveyi*, and *Vibrio parahaemolyticus*, and the probiotic *Lactobacillus acidophilus* were provided by the Key Laboratory of Bioprocess and Biochemical Synthesis Engineering, Institute of Biology, VAST. All the chemicals used in this study, including tetracycline (99%) and oxytetracycline hydrochloride (95%) were purchased from Sigma-Aldrich (St. Louis, MO, USA), while the Rifampicin (95%) was purchased from bioWorld (Dublin, Ohio, US). The de Man–Rogosa–Sharpe (MRS) and Luria–Bertani medium (LB, Sigma-Aldrich, UK) were used to culture the *E. coli* and *L. acidophilus* bacteria, respectively. The pathogens, *V. harveyi* and *V. parahaemolyticus*, were activated in the thiosulfate citrate bile salts sucrose agar plate (TCBS, Sigma-Aldrich, UK), then were aerobically inoculated in LB medium until reaching a desired bacterial density. The MRS medium contains (g L^{-1}): peptone (10), meat extract (10), yeast extract (5), glucose (20), K_2HPO_4 (2), NH_4Cl (2), CH_3COONa (5), $MgSO_4$ (0.2), $C_6H_{17}N_3O_7$ (5), tween (80–100 μl), pH–6.5.

In the current study, the photocatalytic activity of the TiO_2–Ag/EC was assessed under the natural sunlight irritation at the Institute of Biology (VAST), which is located at 21°02′57.2″N 105°48′06.8″E. The experiments were conducted during the time of July to September with the measured light density ranging from 70 to 100 klux, and temperature of 30 to 35 °C.

Optimizing the immobilization of TiO_2–Ag into expanded clay carrier

The expanded clay material (EC) and TiO_2–Ag photocatalyst were prepared using the method outlined in a previous study by Hoang *et al.*[11] The properties of the EC carrier, including surface areas, pore volume, and pore size, were examined using N_2 physisorption isotherms at 77 K (Tristar-3030 system, Micromeritics-USA). The EC material was then rinsed with water and dried at 60 °C for 5 hours to eliminate dirt and impurities. Subsequently, TiO_2–Ag particles were dispersed in a 0.05% alginate solution with varying titanium concentrations (20 000, 25 000, 30 000, or 35 000 ppm). EC was then added to glass beakers containing the prepared TiO_2–Ag solutions at a mass ratio of 1 : 2 (w/v). During the integration process of TiO_2–Ag onto EC, the beakers were magnetically stirred at 100 rpm. After 6, 12, or 18 hours, the EC material was separated from the solution by filtration and subsequently dried at 60 °C for another 5 hours. The titanium and silver content integrated into the EC material (TiO_2–Ag/EC) was analyzed by the inductively coupled plasma mass spectrometry (ICP-MS, ICP Mass Spectrometer, Nexion 2000, PerkinElmer, USA) and the energy-dispersive X-ray spectroscopy (EDX) analysises (Hitachi S-4800 FE-SEM equipped with a Bruker Quantax EDS syste). Based on the results, a comparison was made to determine the optimal initial concentration of the TiO_2–Ag solution and the integration time to achieve the highest integration efficiency.

Measurement of hydrogen peroxide formation by the TiO_2–Ag/EC material

The TiO_2–Ag/EC (3 g) material was added to a 50 mL beaker containing 30 mL of deionized water (HI70346, Hanna Instruments, USA). The beakers were irradiated under sunlight for 4 hours. At the end of each hour, a sample was collected to measure the concentration of hydrogen peroxide formed at 230 nm using a quartz cuvette (UV-1601 Spectrophotometer, SHIMADZU, Japan).[12] The negative control consisted of beakers without any added material. After the first cycle, the material was collected and air-dried at room temperature for approximately 24 hours before being reused in subsequent tests. The

Open Access Article. Published on 02 June 2025. Downloaded on 5/21/2026 6:09:23 AM. This article is licensed under a Creative Commons Attribution-NonCommercial 3.0 Unported Licence.

experiment was conducted in triplicate and repeated for a total of 10 cycles.

Anti-pathogen activity of TiO_2–Ag/EC material

The antibacterial activity of the TiO_2–Ag integrated EC material (TiO_2–Ag/EC) was evaluated against several pathogenic bacteria, including *Vibrio harveyi*, *Vibrio parahaemolyticus*, and *Escherichia coli*. The biomass of these bacterial strains was separately dissolved in a sterile saline solution (0.9% NaCl) to achieve a bacterial density of 10^6 CFU mL^{-1}. TiO_2–Ag/EC particles were then added to each transparent glass vial containing 5 mL of the prepared bacterial solutions. For comparison, an experimental vial containing EC material without TiO_2–Ag integration served as the negative control. After 2 hours of exposure to sunlight, samples were collected to measure the remaining bacterial density in the vials, allowing us to determine the antibacterial effectiveness of the TiO_2–Ag/EC material. The antibacterial effectiveness (A) was calculated using the following formula, where N_0 and N_t represent the bacterial densities before and after treatment with TiO_2–Ag/EC, respectively.

$$A = \log N_0 - \log N_t = \log(N_0/N_t)$$

Following each experiment, the TiO_2–Ag/EC material was gently rinsed with water and left to air dry at room temperature for approximately 24 hours before being reused in subsequent tests. The experiment was repeated over seven cycles using the same method to assess the stability of the material's antibacterial activity.

Antibiotic degradation ability of TiO_2–Ag/EC material

The photocatalytic degradation capability of the TiO_2–Ag/EC material was assessed using three types of antibiotics: tetracycline (TET), oxytetracycline (OTC), and rifampicin (RIF). Reaction solutions were prepared for each antibiotic at varying concentrations (10, 20, and 30 ppm) and pH values (3, 5, 7, and 9). To initiate the experiment, three grams of the TiO_2–Ag/EC material were added to 30 mL of the antibiotic solution and stirred gently in the dark for 30 minutes to reach an equilibrium adsorption state. After this period, the mixture was exposed to sunlight for 4 hours. During the experiment, samples were taken at 1, 2, 3, and 4 hours to measure the remaining concentrations of TET, OTC, and RIF. The concentrations were determined using optical methods at specific UV wavelengths: 354 nm for TET,[13] 352 nm for OTC,[14] and 335 nm for RIF.[15] In the negative control, EC material without TiO_2–Ag was included in the reaction solution. The degradation efficiency of the antibiotics (H) was calculated using the following formula:

$$H\,(\%) = ((C_0 - C_t)/C_0) \times 100\%$$

where C_0 represents the initial concentration of the antibiotic, and C_t is the remaining concentration of the antibiotic in the reaction vial at time t.

The stability of the TiO_2–Ag/EC material for degrading the antibiotic tetracycline was evaluated at an initial concentration of 10 ppm and a pH of 7. After the first cycle, the material was collected and air-dried at room temperature for approximately 24 hours before being reused in subsequent tests. The experiment was conducted in triplicate and repeated for a total of 10 cycles.

Kinetic study on the antibiotics photocatalytics degradation process

Furthermore, the degradation kinetics of each tested antibiotic were analyzed using a pseudo-first-order (PFO) kinetic model, expressed by the equation:

$$\ln(C_0/C_t) = kt$$

where k denotes the reaction rate constant for antibiotic degradation.

Toxicity of photo-catalytically degraded antibiotic solutions on bacterial growth

In this study, the effect of photocatalytically degraded antibiotic solutions on bacterial growth was examined. The biomass of the probiotic *Lactobacillus acidophilus* and the pathogen *Vibrio parahaemolyticus* was prepared at a concentration of 10^5 CFU mL^{-1} and added (2% v/v) to Eppendorf tubes containing 100 μL of the appropriate growth media for each bacterial strain, specifically MRS and LB. Then, antibiotic solutions of tetracycline (TET), oxytetracycline (OTC), and rifampicin (RIF) (10 ppm, pH 7) after degradation by TiO_2–Ag/EC, labeled as TET_{TA}, OTC_{TA}, and RIF_{TA}, were diluted using MRS or LB medium and added to each bacterial tube at different antibiotic concentrations: 0, 5, 10, 15, 20, 25, and 30% (v/v).

Additionally, control groups were established where the bacterial tubes were supplemented with either: (1) antibiotic solutions that were photodegraded under light using a material that did not contain TiO_2–Ag, labeled as TET_{EC}, OTC_{EC}, and RIF_{EC}, or (2) the original TET, OTC, and RIF solutions at a concentration of 10 ppm, pH 7. These were included for comparison with the effects observed from the TET_{TA}, OTC_{TA}, and RIF_{TA} solutions on bacterial growth. The tubes without any added antibiotics served as the negative control.

The experimental model is illustrated in Fig. S1.† After 24 hours of incubation at 35 °C, samples were collected to measure the optical density (OD) of the bacterial solutions at 600 nm. The experimental tubes containing antibiotics that exhibited significantly different ($p < 0.05$) lower OD_{600} values compared to the negative control were determined to have reached the minimum inhibitory concentration necessary to inhibit bacterial growth.

COD removal capacity of TiO_2–Ag/EC material

A stock solution with a chemical oxygen demand (COD) concentration of 250 mg L^{-1} was prepared by adding shrimp feed (Tomboy, Skretting Vietnam) to distilled water at a 0.07% w/v ratio, followed by sterilization.[16] This stock solution was used to simulate aquaculture environments with varying organic contamination levels (25, 50, and 100 mg L^{-1}). TiO_2–Ag/

© 2025 The Author(s). Published by the Royal Society of Chemistry

Open Access Article. Published on 02 June 2025. Downloaded on 5/21/2026 6:09:23 AM. This article is licensed under a Creative Commons Attribution-NonCommercial 3.0 Unported Licence.

EC material was then added to each COD solution at a 10% w/v concentration. The samples were exposed to sunlight for 8 hours daily, from 8:30 AM to 4:30 PM. After each 8 hours exposure period, samples were collected to measure the remaining COD concentration in the environment, following the method outlined by LaPara *et al.*[17] The efficiency of COD removal was calculated using the following equation:

$$\text{Degradation efficiency (\%)} = ((C_0 - C_t)/C_0) \times 100\%$$

where C_0 is the initial COD concentration at the beginning of the experiment, and C_t is the remaining COD concentration in the reactor at time t.

To assess the impact of the TiO_2–Ag/EC material addition ratio on treatment efficiency, six transparent glass beakers were prepared, each containing 1 liter of a solution with a COD concentration of 100 mg L^{-1}. Different ratios of TiO_2–Ag/EC material (0.5%, 1%, 2.5%, 5%, and 7.5% w/v) were added to each beaker, and the photocatalytic degradation process was carried out under sunlight. Samples were collected to measure the remaining COD, ammonia, and nitrite concentrations in the environment after each 8 hours exposure period. Based on the obtained results, the appropriate concentration of photocatalytic material addition was selected to achieve high COD degradation efficiency.

Results and discussion

Optimizing the immobilization of TiO_2–Ag on expanded clay carrier

In this study, the synthesized TiO_2–Ag were uniformly dispersed in the alginate polymer solution. During this synthesis process, the long chains of the alginate polymer envelop the nanoparticles, which not only enhances the stability of the material system but also plays a vital role in the subsequent integration of TiO_2–Ag onto the EC carrier.

When the EC is introduced into the prepared nanoparticle solution, the stirring during the integration process causes the alginate chains, which are bound to the TiO_2–Ag nanoparticles, to continue surrounding the EC (Fig. 1a). The Brunauer–Emmett–Teller analysis indicated that the original EC has a total surface area of 2.41 m^2 g^{-1}, displaying moderate mesoporosity with an average pore diameter ranging from 8 to 18 nm, along with minimal microporosity. These properties suggest that the outer porous structure of the EC offers optimal docking sites for the nanoparticles, facilitating efficient integration (Fig. S2†). As the TiO_2–Ag solution concentration increased from 20 000 ppm to 35 000 ppm, and the integration time extended from 6 to 12 to 18 hours, more nanoparticles were incorporated into the EC's surface pores. The integration efficiency peaked at a TiO_2–Ag concentration of 35 000 ppm, with the Ti density on the EC reaching its maximum of 2503.95 ± 35.80 ppm after 12 hours. No further increase in Ti content was observed when the integration time was extended to 18 hours (Fig. 1b and Table 1). Additionally, the EDX results clearly demonstrate that the original EC carrier contains a low Ti content of 0.51 ± 0.11% and does not include any silver. In contrast, the Ti content in the fabricated TiO_2–Ag/EC significantly increases to 17.22 ± 1.80%, while the Ag content rises to 0.75 ± 0.12%. Furthermore, the immobilization of TiO_2–Ag nanoparticles enhances the total surface area of TiO_2–Ag/EC to 3.17 m^2 g^{-1} (Fig. S2 and S3†). The distribution of TiO_2–Ag nanoparticles on the EC carrier can be observed in the FESEM images at various magnifications (Fig. 2).

In similar research, Kaur *et al.* optimized the integration of TiO_2 onto clay beads for the degradation of the fungicide carbendazim.[18] Though the exact Ti content integrated into the support was not specified, the authors found that an initial TiO_2 concentration of 20 000 ppm, with two integration steps over 24 hours, resulted in the thickest TiO_2 layer. However, no further increase in TiO_2 thickness occurred after repeating the integration. In contrast, the present study found that the integration of TiO_2–Ag reached saturation much more quickly, after just one 12 hours integration step with an initial TiO_2–Ag concentration of 35 000 ppm. The difference may arise from the uniform dispersion of TiO_2–Ag within the alginate and the continuous stirring that occurred during the integration process in this study, contrasting with the static condition of

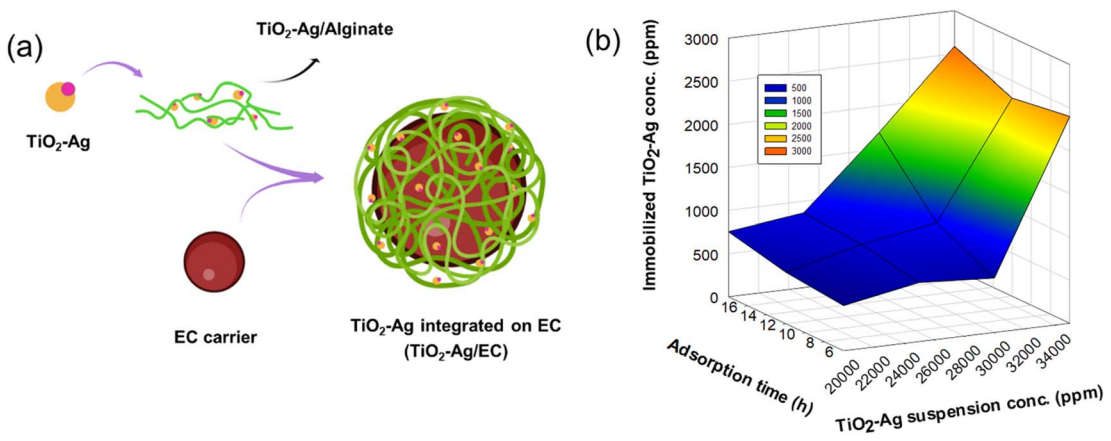

Fig. 1 Integration mechanism of TiO_2–Ag onto an expanded clay carrier (a) and impact of integration time and concentration on the immobilization of TiO_2–Ag on the EC carrier (b).

Open Access Article. Published on 02 June 2025. Downloaded on 5/21/2026 6:09:23 AM. This article is licensed under a Creative Commons Attribution-NonCommercial 3.0 Unported Licence.

Table 1 Variation in Ti and Ag concentrations immobilized on EC under varying time and TiO_2–Ag concentration conditions

			Ti (ppm)	Ag (ppm)
Original EC			38.94 ± 5.32	—
Ti content in TiO_2–Ag	Time	Sample	Ti content on EC (ppm)	Ag content on EC (ppm)
20 000 ppm	6 h	TiO_2–Ag/$EC_{6–20k}$	524.32 ± 63.21	154.47 ± 24.74
	12 h	TiO_2–Ag/$EC_{12–20k}$	597.26 ± 20.40	132.63 ± 37.65
	18 h	TiO_2–Ag/$EC_{18–20k}$	755.85 ± 28.53	133.66 ± 8.12
25 000 ppm	6 h	TiO_2–Ag/$EC_{6–25k}$	685.36 ± 10.06	306.71 ± 63.58
	12 h	TiO_2–Ag/$EC_{12–25k}$	814.33 ± 30.11	116.71 ± 2.76
	18 h	TiO_2–Ag/$EC_{18–25k}$	864.63 ± 6.79	226.00 ± 39.93
30 000 ppm	6 h	TiO_2–Ag/$EC_{6–30k}$	631.09 ± 89.44	354.75 ± 34.21
	12 h	TiO_2–Ag/$EC_{12–30k}$	957.00 ± 52.95	405.17 ± 52.73
	18 h	TiO_2–Ag/$EC_{18–30k}$	1198.60 ± 42.39	350.73 ± 34.85
35 000 ppm	6 h	TiO_2–Ag/$EC_{6–35k}$	1691.25 ± 19.02	793.5 ± 92.62
	12 h	TiO_2–Ag/$EC_{12–35k}$	2503.95 ± 35.80	961.62 ± 54.55
	18 h	TiO_2–Ag/$EC_{18–35k}$	2584.51 ± 49.52	332.45 ± 23.85

the TiO_2 nanoparticles during the integration process described by Kaur *et al.*[18] This study investigated a novel strategy for improving TiO_2–Ag nanoparticles' immobilization efficiency. The approach emphasizes two principal factors. First, alginate chains function as an effective matrix for coating the porous surface of the EC carrier, facilitated by water flow induced through mechanical stirring. However, careful optimization of stirring speed is required to prevent excessive shear stress, which may lead to detachment of the immobilized TiO_2–Ag nanoparticles from the carrier surface. Overall, the results demonstrate that the immobilization efficiency is governed by multiple parameters, including the physicochemical properties and concentration of TiO_2–Ag, as well as the morphological characteristics of the EC carrier.

Previously, various methods have been employed in previous research to integrate photocatalytic substances into materials, including high-temperature treatment, sol-spray coating, electrodeposition, chemical vapor deposition (CVD), and dip-coating.[19] Electrodeposition, for example, allows for the formation of photocatalytic layers with controllable thicknesses tailored to specific structures.[20] Dunlop *et al.* used electrodeposition to coat semiconductor materials with TiO_2 under an electric current and subsequently heated them at 500 °C to enhance stability.[21] Similarly, thermal treatment is a common method for integrating TiO_2 onto carriers, with annealing temperatures around 400 °C promoting the transformation of TiO_2 from anatase to rutile, a more stable form.[22] However, these techniques, though efficient, are impractical for aquaculture applications due to the significant costs and sophisticated equipment required.

Hydrogen peroxide formation by the TiO_2–Ag/EC photocatalytic activity

TiO_2–Ag nanoparticles exhibit enhanced reactive oxygen species (ROS) formation activity under visible light compared to TiO_2 alone, primarily due to the localized surface plasmon resonance effect of the silver nanoparticles.[23] One of the major ROS compounds generated by TiO_2–Ag is hydrogen peroxide (H_2O_2). During sunlight irradiation, electrons from the conduction band can reduce O_2 to produce H_2O_2. However, to date, the resultant product concentrations have been limited in study.

In this research, TiO_2–Ag immobilized on electrospun composite (EC) material was tested for its H_2O_2 production ability. The results, presented in Fig. S4,† showed that H_2O_2 concentration increased with irradiation time, reaching a peak value of approximately 280 mM after 4 hours. The material demonstrated highly stable H_2O_2 production, maintaining

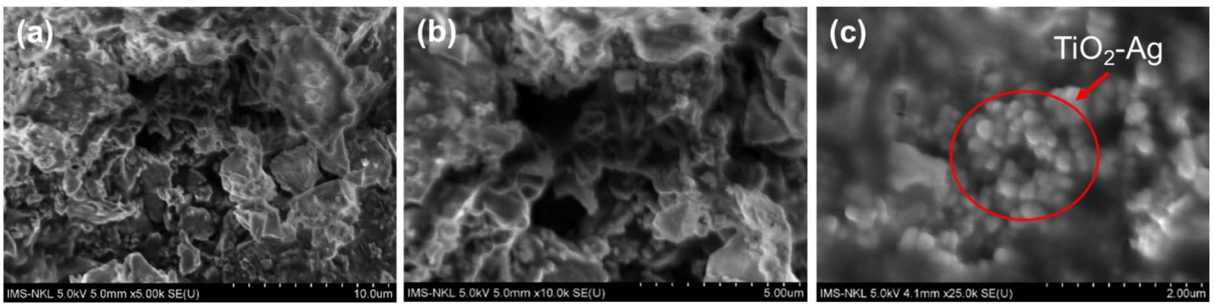

Fig. 2 FESEM images of TiO_2–Ag nanoparticles integrated on EC materials at magnifications of 5 k (a), 10 k (b), and 25 k (c).

© 2025 The Author(s). Published by the Royal Society of Chemistry

Open Access Article. Published on 02 June 2025. Downloaded on 5/21/2026 6:09:23 AM. This article is licensed under a Creative Commons Attribution-NonCommercial 3.0 Unported Licence.

a concentration of 266.22 ± 13.42 mM even after being continuously tested for 10 cycles. These results provide evidence of the photocatalytic activity of the TiO_2–Ag/EC material.

Antibacterial activity of TiO_2–Ag/EC

The prolonged overuse of antibiotics for disease prevention and treatment presents significant risks to both environmental and human health. A comprehensive review of studies published from 2002 to 2023 by Suyamud *et al.* identified three pathogenic bacterial genera, including *Escherichia coli*, *Aeromonas*, and *Vibrio* as the common carriers of antibiotic resistance genes within aquaculture systems.[3] In recent years, photocatalytic materials have gained significant attention for their promising ability to eliminate pathogenic bacteria. Typically, TiO_2 materials require UV light to excite electrons from the valence band to the conduction band, generating highly reactive oxygen species (ROS) radicals. However, in this study, Ag-modified TiO_2 nanoparticles were employed to enhance the visible light absorption ability of the material. After two hours of sunlight exposure, the TiO_2–Ag/EC material successfully inactivated *V. parahaemolyticus*, *V. harveyi*, and *E. coli* pathogens, reducing their concentrations from approximately 10^6 CFU mL^{-1} to 7, 68, and 12 CFU mL^{-1}, respectively. These reductions correspond to antibacterial efficiencies of 6.0, 5.1, and 5.8 log reductions (N_0/N_t), as shown in Fig. 3. A study by Zhang *et al.* also examined the use of TiO_2–Ag integrated into a ceramic carrier to inhibit *E. coli* pathogens. However, after a 2 hours irritation, the material achieved only a 2–3 log reduction in bacterial count, which is significantly lower than the effectiveness of the TiO_2–Ag/EC material (Table 2).

To enhance the reuse of TiO_2–Ag/EC, the materials were gently rinsed with distilled water and air-dried in the dark at room temperature before undergoing further testing. The results showed that after four cycles of reuse, the TiO_2–Ag/EC material retained substantial antibacterial activity, achieving an efficiency of over a 4 log reduction (N_0/N_t) against *V. parahaemolyticus* and *V. harveyi* (Fig. 3). Although the antibacterial efficiency gradually decreased from 5.1–6.0 log reductions to 2.5–3.2 log reductions (N_0/N_t) at the 7th reuse, the material remained highly effective at eliminating pathogenic bacteria. It reduced bacterial concentrations from 10^6 CFU mL^{-1} to approximately 10^3 CFU mL^{-1} within just 2 hours of treatment. The antibacterial performance of TiO_2–Ag/EC is comparable to other materials, such as TiO_2/Ag/Ni films,[23] Mn- and Co-doped TiO_2,[28] and TiO_2 nanoparticles encapsulated in cellulose acetate films,[26] as previously reported (Table 2).

Additionally, Joost *et al.* have suggested that during photocatalysis, reactive oxygen species (ROS) disrupt bacterial cell integrity, leading to the leakage of intracellular components. While titanium dioxide (TiO_2) can kill bacteria within 20 minutes, electron microscopy reveals that cell debris may persist on the surface even after 60 minutes of treatment.[29] These residual debris can hinder light absorption and block the active sites of the photocatalyst, thereby diminishing its efficacy upon reuse.[29,30] Therefore, after bacterial inactivation by TiO_2, prolonging the reaction time is essential to ensure complete degradation of the cell components. Besides, methods such as heating, ultrasonic treatment, or the use of basic solutions can effectively eliminate accumulated impurities, thus regenerating the surface of the photocatalyst for future applications.[31] Cao *et al.* reported that heating TiO_2 to 420 °C was required to

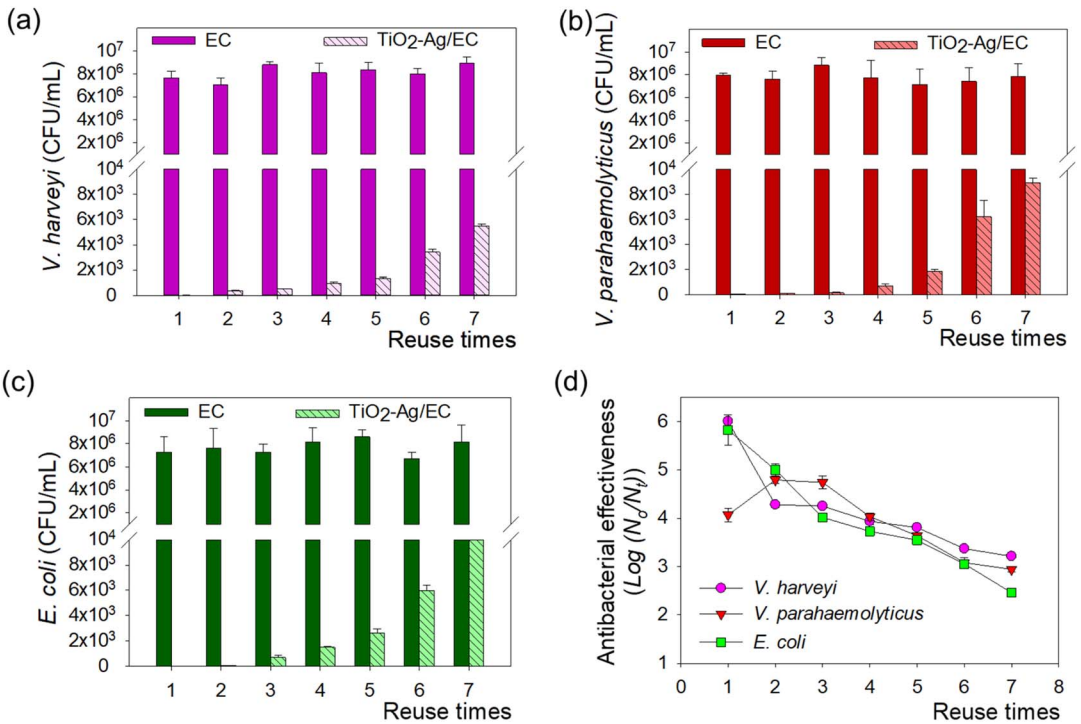

Fig. 3 Pathogen inhibition ability of TiO_2–Ag/EC against *V. harveyi* (a), *V. parahaemolyticus* (b), *E. coli* (c), and TiO_2–Ag/EC antibacterial efficacy (d).

Open Access Article. Published on 02 June 2025. Downloaded on 5/21/2026 6:09:23 AM.
This article is licensed under a Creative Commons Attribution-NonCommercial 3.0 Unported Licence.

Table 2 Comparison of antibacterial efficacy of TiO_2–Ag/EC with the synthesized photocatalyst agents in other studies

Photocatalyst agent	Light source	Initial pathogen density (CFU mL^{-1})		Irritation time	Pathogen strain	Antibacterial activity $\log(N_0/N_t)$	Reference
TiO_2–Ag/EC	Natural sunlight	7.7×10^6	1st	120 min	*V. harveyi*	6.0 log	The presence study
		8.9×10^6	7th			3.2 log	
		8.0×10^6	1st		*V. parahaemolyticus*	5.1 log	
		7.8×10^6	7th			2.9 log	
		7.2×10^6	1st		*E. coli*	5.8 log	
		8.2×10^6	7th			2.5 log	
Ag/TiO_2-functionalized ceramic tiles	Xenon lamp (1000 W; $\lambda \geq 420$ nm)	1×10^6		120 min	*E. coli*	2–3 log	Zhang *et al.*[22]
					S. aureus	2–3 log	
					Salmonella	2–3 log	
					Shigella	2–3 log	
Face masks coated with 2% TiO_2	Natural sunlight	10^5		18 h	*E. coli*	3.7 log	Ahmed *et al.*[24]
					S. aureus	3.34 log	
Plastic cutting board coated with TiO_2	UV-A lamp (λ_{max} ~356 nm)	10^7		180 min	*E. coli*	2.67 log	Yemmireddy *et al.*[25]
TiO_2 -embedded cellulose acetate film	UV-A lamp (λ_{max} ~356 nm)	1×10^7		360 min	*E. coli*	5.2 log	Xie *et al.*[26]
TiO_2/Ag/Ni film	UV	7.2×10^4		10 min	*P. fluorescens*	2.48 log	Skorb *et al.*[23]
2 wt% Ni/TiO_2 mesh	UV-A lamp	1×10^7		30 minn	*E. coli*	5.17 log	Jeong *et al.*[27]
Mn- and Co-doped TiO_2	Xenon (with 5% of UV-A and 0.1% of UV-B light)	1.5×10^8		60 min	*K. pneumoniae*	6 log	Venieri *et al.*[28]
	Natural sunlight					3 log	

© 2025 The Author(s). Published by the Royal Society of Chemistry

Open Access Article. Published on 02 June 2025. Downloaded on 5/21/2026 6:09:23 AM. This article is licensed under a Creative Commons Attribution-NonCommercial 3.0 Unported Licence.

remove all organic compounds adsorbed during the toluene degradation process.[32] In contrast, the present study demonstrated that simple water rinsing was sufficient to preserve the antibacterial activity of TiO_2–Ag/EC after seven uses, emphasizing the ease of use of the material for preventing pathogen spread in aquaculture systems.

Antibiotics photodegradation activity of TiO_2–Ag/EC

The excessive accumulation of antibiotics in the environment has led to the emergence of antibiotic-resistant genes and bacteria. Thus, this study assessed the TiO_2–Ag/EC material not only for its capacity to inhibit pathogenic bacteria but also for its effectiveness in degrading several widely used antibiotics in aquaculture, including tetracycline (TET), oxytetracycline (OTC), and rifampicin (RIF). During the treatment process, the TiO_2–Ag/EC material was introduced to an antibiotic solution and allowed to remain static in the dark for 30 minutes to achieve adsorption equilibrium, followed by exposure to natural sunlight for photocatalytic degradation. The environmental pH and initial antibiotic concentrations were identified as critical factors influencing degradation efficiency. Thus, the degradation process was evaluated at four pH levels (3, 5, 7, and 9) and three antibiotic concentrations (10, 20, and 30 ppm).

TiO_2–Ag typically exhibits an isoelectric point (pH_{pzc}) of 6.6. Hence, at pH levels below this threshold, the material possesses a positive surface charge, whereas at pH values above 6.6, it acquires a negative charge.[33] Tetracycline (TET) and oxytetracycline (OTC) are classified as amphoteric substances, possessing the capability to both donate and accept protons. Moreover, the two antibiotics display similar pK_a values: pK_{a1} ranges from 3.27 to 3.30, pK_{a2} from 7.32 to 7.68, and pK_{a3} from 9.11 to 9.69.[34] At pH levels either below 3 or above 9, TET, OTC, and TiO_2–Ag all exhibit the same charge, which leads to electrostatic repulsion and consequently limits the degradation processes. According to Sun *et al.* reactive oxygen species (ROS) have short lifespans and are easily decomposed as they move away from the photocatalyst surface.[35] Therefore, it is crucial to maintain close binding of pollutants to the TiO_2–Ag/EC surface to accelerate the photocatalytic reaction rate.

As the pH increases from 3 to 7, the positive charge on TiO_2–Ag decreases, while TET and OTC become neutral, reducing electrostatic repulsion and significantly enhancing degradation efficiency. For example, at pH 3, degradation efficiency for TET and OTC was 86.9–89.6%, which increased to 92.3–95.1% at pH 7, with an initial antibiotic concentration of 10 ppm. At pH levels of 7–9, the antibiotic compounds and TiO_2–Ag carry negative charges, however, the charge density of both components may still be low, allowing degradation efficiency to remain high, reaching 94.6% for TET and 97.8% for OTC (Fig. 4 and 5).

In the photocatalytic degradation process of TET and OTC, it is suggested that the reactive oxygen species (ROS) produced by TiO_2–Ag initiate oxidative reactions such as hydroxylation, quinonization, decarbonylation, demethylation, and dehydration. These reactions lead to the cleavage of carbon–carbon (C–

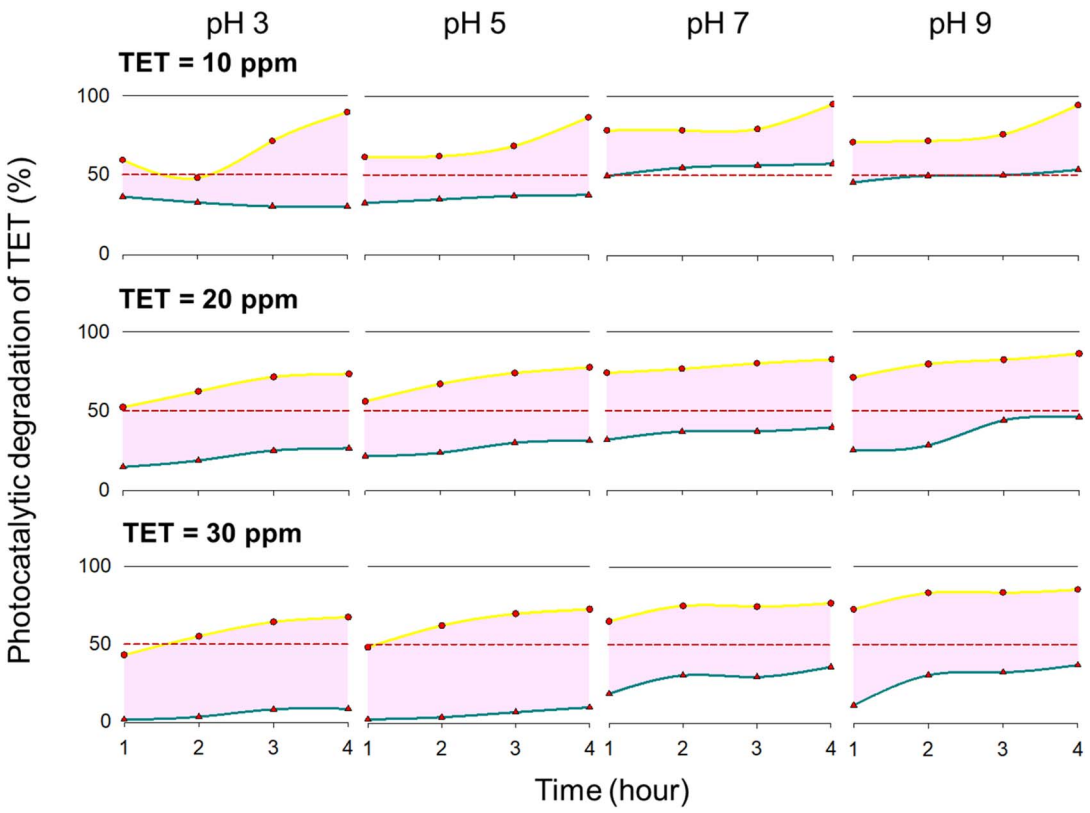

Fig. 4 Photodegradation of tetracycline (TET) by TiO_2–Ag/EC material at various environmental pH and initial antibiotics concentrations.

Open Access Article. Published on 02 June 2025. Downloaded on 5/21/2026 6:09:23 AM.
This article is licensed under a Creative Commons Attribution-NonCommercial 3.0 Unported Licence.

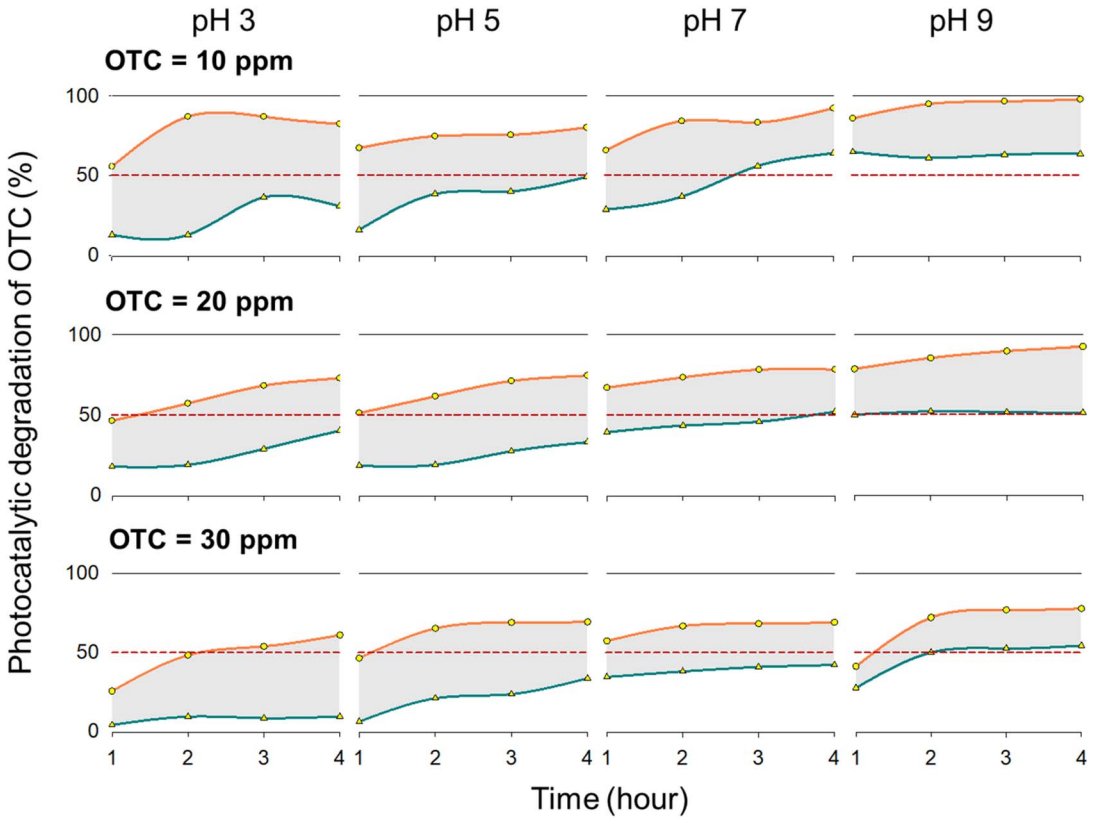

Fig. 5 Photodegradation of oxytetracycline (OTC) by TiO_2–Ag/EC material at various environmental pH and initial antibiotics concentrations.

C) and carbon–nitrogen (C–N) bonds, disruption of the fused, linearly connected ring structures of the antibiotics, and ultimately resulting in mineralization of antibiotics into harmless end products like carbon dioxide (CO_2), ammonium (NH_4^+), and water (H_2O).[36]

In case of the rifampicin (RIF), the ROS initially cleave the carbon atom bonded to the amino group, triggering demethylation. This process breaks the tetrahydrofuran ring, resulting in mineralization into CO_2 and H_2O.[37] The RIF has the two pK_a values of 1.7 and 7.9.[38] As the pH shifts from 3 to 5, RIF becomes neutral, while the positive charge on TiO_2–Ag decreases, enhancing the binding of RIF to the photocatalyst and resulting in a degradation efficiency of 95.7%. However, RIF degradation is inhibited at higher pH values. At pH 7, 76.7% of the initial RIF concentration (10 ppm) was degraded after 4 hours, while this decreased to 69.9% at pH 9 (Fig. 6).

Simultaneously with the photocatalytic process, antibiotics can directly absorb photons, which alters their chemical structures and contributes to their degradation.[39] Compounds with alternating saturated and unsaturated bonds, such as TET, OTC, and RIF, are more likely to undergo direct photon absorption.[40] The results showed that the photolysis process could degrade 53.7% to 63.6% of TET and OTC at an initial concentration of 10 ppm (Fig. 4 and 5). However, as the antibiotic concentration increased to 20 or 30 ppm, the photolysis efficiency dropped below 50%. Rifampicin is more resistant to degradation in the absence of TiO_2–Ag/EC. At a concentration of 10 ppm (pH 7), only 15.7% of the initial RIF was removed after 4 hours of photolysis, while the addition of TiO_2–Ag/EC increased the degradation efficiency to 76.7% (Fig. 6). The obtained results consistent with findings from Dai *et al.*, which reported lower photolysis efficiency for TET degradation compared to photocatalytic treatments.[41] Research by Zambrano *et al.* further emphasizes the effectiveness of TiO_2 in antibiotic degradation, revealing that several antibiotics, including tetracycline, ciprofloxacin, sulfadiazine, and sulfamethoxazole, take 100 to 240 hours to degrade under UV-C exposure, while TiO_2 enhanced the degradation efficiency to 99–100% in just 3.5 to 15.6 hours.[42] These findings proved the critical role of TiO_2–Ag/EC in improving the efficiency of antibiotic degradation, highlighting its potential for addressing residual antibiotics in the environment.

To evaluate the stability and reusability of the TiO_2–Ag/EC catalyst, we conducted repeated cycles of tetracycline (TET) degradation under identical conditions, initial concentration of 10 ppm at neutral pH (7.0), for up to 10 cycles. As shown in Fig. S5,† the catalyst maintained over 80% removal efficiency for the first six cycles. However, a noticeable decline was observed, with efficiency dropping to below 40% by the 10th cycle.

Interestingly, this decrease in activity does not appear to be associated with the relatively stable concentrations of H_2O_2 produced by TiO_2–Ag/EC in deionized water, as illustrated in Fig. S4.† This suggests that the diminished photocatalytic efficiency may be more related to surface fouling, likely caused by the adsorption of intermediate degradation products rather than to catalyst leaching.

© 2025 The Author(s). Published by the Royal Society of Chemistry

Open Access Article. Published on 02 June 2025. Downloaded on 5/21/2026 6:09:23 AM.
This article is licensed under a Creative Commons Attribution-NonCommercial 3.0 Unported Licence.

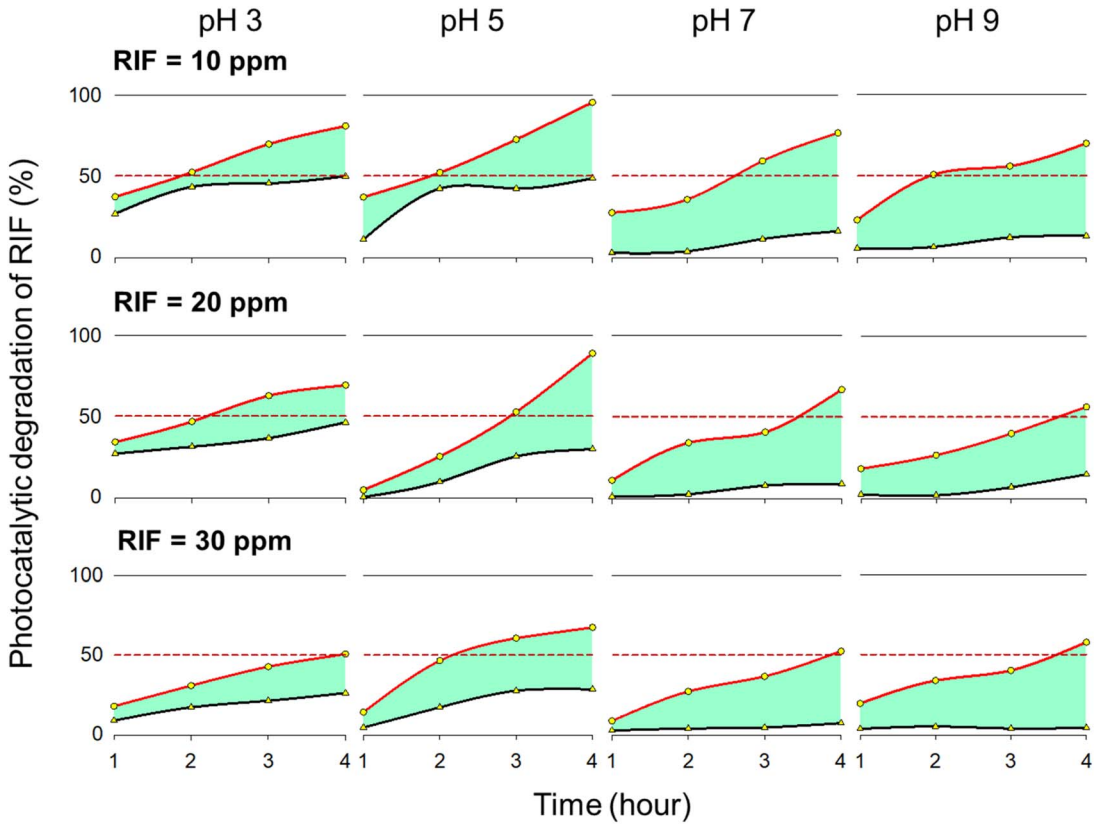

Fig. 6 Photodegradation of rifampicin (RIF) by TiO_2–Ag/EC material at various environmental pH and initial antibiotics concentrations.

Although we did not directly measure TiO_2–Ag leaching in this study, the immobilized nature of the TiO_2–Ag on the EC carrier and the consistent ROS generation imply minimal catalyst loss. For practical applications, it is recommend further enhancing catalyst stability by applying a chitosan coating to the TiO_2–Ag/EC material. Chitosan is poorly soluble at neutral pH, such as that found in aquaculture environments, and could help prevent the detachment of TiO_2–Ag without compromising photocatalytic activity.[43]

Kinetic study on the antibiotics photocatalytics degradation process

To further investigate the degradation of these antibiotics by TiO_2–Ag/EC, the kinetics of the process using the pseudo-first-order (PFO) kinetic model was also analyzed. The R^2 values for all models ranged from 0.87 to 0.99, showing a good fit for the experimental data. The degradation rate constants (k) for TET, OTC, and RIF at a concentration of 20 ppm under different pH conditions are shown in Fig. S2† and Table 3. Specifically, the rate constants for TET and OTC increased from 5.45×10^{-3} and 5.53×10^{-3} at pH 3 to their highest values of 10.83×10^{-3} and 8.31×10^{-3} at pH 9, which correlates with the increased degradation efficiency that was observed under basic conditions. In contrast, RIF degradation was most efficient in mildly acidic conditions, pH 5, with the highest rate constant of 9.23×10^{-3}.

Table 3 The rate constant (k) and R^2 value for antibiotic degradation using TiO_2–Ag/EC material under sunlight

	Oxytetracycline		Tetracycline		Rifampicin	
	k	R^2	k	R^2	k	R^2
pH 3	5.45×10^{-3}	0.99	5.53×10^{-3}	0.95	4.92×10^{-3}	0.97
pH 5	5.71×10^{-3}	0.98	6.24×10^{-3}	0.98	9.23×10^{-3}	0.87
pH 7	6.40×10^{-3}	0.90	7.30×10^{-3}	0.99	4.58×10^{-3}	0.92
pH 9	10.83×10^{-3}	0.99	8.31×10^{-3}	0.98	3.45×10^{-3}	0.95

Impact of degraded antibiotic solutions on the growth of bacteria

The addition of probiotics, particularly *Lactobacillus* species, to aquaculture environments or feeds is commonly used to enhance digestion, growth performance, and overall productivity. However, the growth of *Lactobacillus* is sensitive to environmental factors, as it is a non-spore-forming bacterium.[44] Therefore, this study aimed to evaluate the effectiveness of photocatalytic and photolysis processes in reducing the toxicity of residual antibiotics on the growth of *Lactobacillus acidophilus*.

Tetracycline (TET) and oxytetracycline (OTC), both members of the tetracycline antibiotic group, have chemical structures with multiple binding sites for metal ions, such as the β-diketone system (C11, C12), enol group (C1, C3), and carboxamide group (C2).[45] These antibiotics form complexes with

Open Access Article. Published on 02 June 2025. Downloaded on 5/21/2026 6:09:23 AM.
This article is licensed under a Creative Commons Attribution-NonCommercial 3.0 Unported Licence.

L. acidophilus

	Antibiotic concentrations						
	0	5%	10%	15%	20%	25%	30%
TET	0.964	0.054	0.048	0.040	0.064	0.048	0.077
TET_{EC}	1.083	0.666	0.069	0.065	0.040	0.045	0.063
TET_{TA}	1.055	1.129	1.139	1.065	1.179	1.054	1.107

	0	5%	10%	15%	20%	25%	30%
OTC	1.178	0.044	0.057	0.070	0.073	0.067	0.059
OTC_{EC}	1.143	0.718	0.305	0.069	0.065	0.040	0.056
OTC_{TA}	0.989	1.140	1.137	1.239	1.088	1.086	1.141

	0	5%	10%	15%	20%	25%	30%
RIF	1.231	0.046	0.065	0.063	0.070	0.058	0.058
RIF_{EC}	1.145	0.079	0.067	0.073	0.068	0.056	0.066
RIF_{TA}	1.204	1.213	1.078	1.145	1.051	1.117	1.118

V. parahaemolyticus

	Antibiotic concentrations						
	0	5%	10%	15%	20%	25%	30%
TET	0.432	0.243	0.066	0.065	0.048	0.060	0.067
TET_{EC}	0.447	0.274	0.074	0.043	0.074	0.038	0.080
TET_{TA}	0.463	0.525	0.507	0.495	0.483	0.539	0.512

	0	5%	10%	15%	20%	25%	30%
OTC	0.520	0.221	0.062	0.046	0.044	0.049	0.074
OTC_{EC}	0.514	0.529	0.249	0.066	0.044	0.025	0.042
OTC_{TA}	0.470	0.524	0.516	0.537	0.540	0.527	0.524

	0	5%	10%	15%	20%	25%	30%
RIF	0.492	0.072	0.072	0.064	0.058	0.048	0.066
RIF_{EC}	0.485	0.148	0.053	0.033	0.025	0.039	0.042
RIF_{TA}	0.512	0.511	0.569	0.590	0.520	0.559	0.553

Fig. 7 Effects of original antibiotics (TET, OTC, and RIF), photolyzed antibiotics (TET_{EC}, OTC_{EC}, and RIF_{EC}), and photocatalytically degraded antibiotics by TiO_2–Ag/EC materials (TET_{TA}, OTC_{TA}, and RIF_{TA}) on the growth of *L. acidophilus* (left) and *V. parahaemolyticus* (right).

magnesium ions (Mg^{2+}), which inhibit protein synthesis in the 30S ribosomal subunit, contributing to their antibacterial effectiveness. In this study, the growth of *L. acidophilus* was completely inhibited at antibiotic concentrations of 5% (0.5 mg mL^{-1}) for both TET and OTC. An increase to 10% concentration also resulted in the inactivation of *V. parahaemolyticus* bacteria. Nevertheless, after 4 hours of photocatalytic treatment using TiO_2–Ag/EC material, over 92% of the TET and OTC content was degraded. As a result, the treated antibiotic solutions, TET_{TA} and OTC_{TA}, lost their ability to inhibit the growth of *L. acidophilus* and *V. parahaemolyticus* at the tested concentrations. At the 30% supplementation level, the growth of bacterial strains in TET_{TA} and OTC_{TA} was comparable to those in the negative control, which contained no antibiotics (Fig. 7).

Yuan *et al.* proposed that reactive oxygen species (ROS) generated during photocatalysis can break the chemical bonds

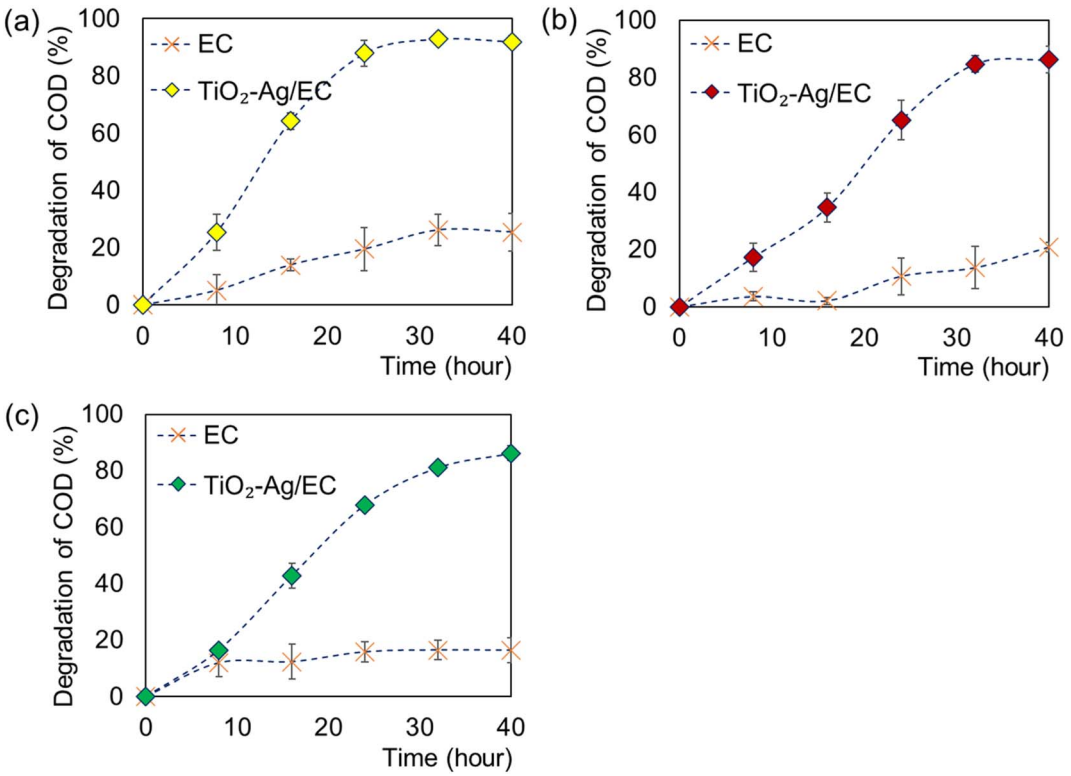

Fig. 8 Dependence of the COD removal activity of TiO_2–Ag/EC on initial COD concentrations: 25 mg L^{-1} (a), 50 mg L^{-1} (b), and 100 mg L^{-1} (c).

© 2025 The Author(s). Published by the Royal Society of Chemistry

Open Access Article. Published on 02 June 2025. Downloaded on 5/21/2026 6:09:23 AM. This article is licensed under a Creative Commons Attribution-NonCommercial 3.0 Unported Licence.

in oxytetracycline (OTC), converting it into harmless byproducts such as 1,4-benzenedicarboxylic acid, 4-oxopentanoic acid, and glycerin.[46] Nevertheless, the intermediate products formed during the photolysis of OTC may have altered functional groups but retained a tetra-phenyl structure, allowing them to penetrate bacterial membranes, including those of luminescent bacterial strains.[47] Furthermore, in the present study, the photolysis of antibiotics in the presence of EC without TiO_2–Ag resulted in only partial degradation of TET and OTC, with efficiencies of 57.5% and 64.0%, respectively (Fig. 4 and 5). As a result, at TET_{EC} and OTC_{EC} concentrations of 15%, the growth of both bacterial strains was effectively inhibited. Similar results were observed with the antibiotic rifampicin (RIF), where *L. acidophilus* was completely inhibited at a concentration of 5% RIF_{EC} but grew normally in the presence of 30% RIF_{TA} (Fig. 7).

COD removal

In addition to the concerns regarding the spread of pathogens and antibiotic residues, the accumulation and subsequent decomposition of excess feed contribute to an increasing concentration of organic matter in the waterbody, which can lead to the deterioration of water quality in the aquaculture environment. The findings presented in Fig. 8 demonstrate that the TiO_2–Ag/EC material (10% w/v) can effectively reduce the initial chemical oxygen demand (COD) concentration of 25 mg L^{-1} by 92.9 ± 0.7% after 32 hours of sunlight exposure. Notably, the removal efficiency remained high, exceeding 86% after 40 hours of treatment when COD concentrations increased to 50 mg L^{-1} and 100 mg L^{-1}. It is worth mentioning that while photolysis of organic compounds occurred under sunlight, the efficiency of this process was relatively lower, at approximately 25.5% across all three tested COD concentrations.

To evaluate the impact of TiO_2–Ag/EC concentration on COD removal efficiency, varying concentrations of TiO_2–Ag/EC, ranging from 0.5% to 10% w/v, were introduced to a 100 mg L^{-1} COD solution. As illustrated in Fig. 9, an increase in TiO_2–Ag/EC concentration from 0.5% to 2.5% w/v resulted in a reduction of the remaining COD from 33.6 ± 5.5 mg L^{-1} to 18.4 ± 3.1 mg L^{-1}, achieving a maximum COD removal efficiency of 82.7 ± 2.0% after 40 hours of illumination. Munien *et al.* revealed that UV illumination with a TiO_2 concentration of 600 ppm can achieve a COD removal rate of 25.88% in domestic wastewater.[48] Additionally, Orojlou *et al.* found a significantly higher COD removal efficiency of 94.5% in industrial

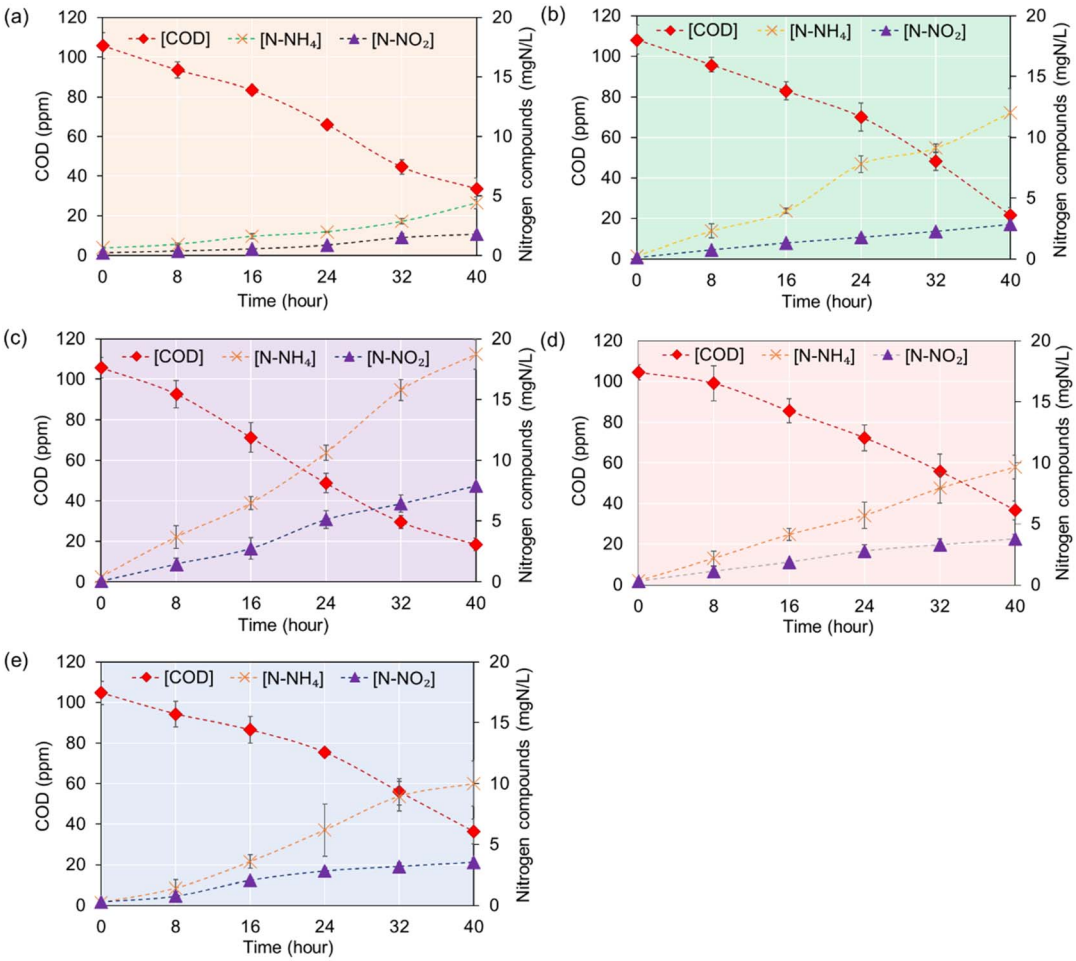

Fig. 9 Effects of various concentrations of TiO_2–Ag/EC additions: 0.5% (a), 1% (b), 2.5% (c), 5% (d), and 7.5% (e) w/v on COD removal efficiency.

Open Access Article. Published on 02 June 2025. Downloaded on 5/21/2026 6:09:23 AM. This article is licensed under a Creative Commons Attribution-NonCommercial 3.0 Unported Licence.

wastewater at an increased TiO_2 concentration of 2000 ppm.[49] In contrast, the TiO_2–Ag/EC composite was synthesized with an integrated Ti content of approximately 2500 ppm, hence, an addition ratio of 2.5% w/v TiO_2–Ag/EC corresponds to a photocatalyst concentration of about 62.5 ppm. Nevertheless, the floatable properties of TiO_2–Ag/EC enhance light absorption and oxygen interaction, thereby improving photocatalytic activity. As a result, this material can achieve a COD removal efficiency exceeding 80% when applied to an initial COD concentration of 100 mg L^{-1} over a treatment period of 40 hours.

However, as the TiO_2–Ag/EC concentration increased to 5% and 7.5% w/v, the efficiency subsequently decreased to 65.2 ± 6.7%. A similar phenomenon was reported by Zhang *et al.*, where the rise in the concentration of the photocatalyst KBNNO ($[KNbO_3]_{0.9}$–$[BaNi_{0.5}Nb_{0.5}O_{3-\delta}]_{0.1}$) from 1800 to 2000 mg L^{-1} did not significantly enhance the removal efficiency of methyl blue dye.[50] This phenomenon can be explained by the fact that at lower photocatalyst densities, the number of photons absorbed and converted into reactive oxygen species (ROS) radicals is limited, resulting in lower degradation efficiency. Conversely, when the photocatalyst concentration exceeds a certain threshold, the nanoparticles may shadow one another, which reduces light absorption and overall photocatalytic activity. Therefore, it is essential to identify the minimum concentration of material needed to achieve effective treatment efficiency for each treatment model to reduce investment costs.

In addition to the COD decomposition process, the formation of inorganic compounds such as NH_4^+ and NO_2^- was observed, with their concentrations increasing over time (Fig. 9). The reactor containing 2.5% w/v TiO_2–Ag/EC demonstrated the most effective performance in degrading organic compounds, resulting in high concentrations of NH_4^+ and NO_2^-, measured at 18.7 ± 1.2 mgN L^{-1} and 7.9 ± 0.2 mgN L^{-1}, respectively. Therefore, a combination of multiple strategies is essential for effectively addressing the nitrogen pollution generated during the degradation of organic compounds in aquaculture systems.

Conclusions

The present study demonstrates the effectiveness of the floatable photocatalyst material, TiO_2–Ag/EC, in addressing environmental issues commonly encountered in aquaculture systems. The integration of the photocatalyst within the EC materials is influenced by both the characteristics and concentration of TiO_2–Ag, as well as the structural features of the material itself. The TiO_2–Ag/EC (10% w/v) material can eliminate pathogenic bacteria such as *Vibrio harveyi*, *Vibrio parahaemolyticus*, and *Escherichia coli* within just 2 hours of sunlight exposure. Moreover, the antibacterial activity of the TiO_2–Ag/EC material remains effective even after seven uses. In addition to its antibacterial properties, TiO_2–Ag/EC has demonstrated the ability to degrade three types of antibiotics: tetracycline, oxytetracycline, and rifampicin. The degradation efficiency varies based on pH conditions and the initial concentrations of the antibiotics. Notably, the floatable properties of TiO_2–Ag/EC enhance light absorption and oxygen interaction, thereby improving photocatalytic activity. With an additional ratio of 2.5% w/v, TiO_2–Ag/EC achieves a COD removal efficiency exceeding 80% when applied to an initial COD concentration of 100 mg L^{-1} over a treatment period of 40 hours. These findings suggest that the TiO_2–Ag/EC material has significant practical potential for improving water quality in the aquaculture system.

Data availability

The data supporting this article have been included as part of the ESI.†

Author contributions

Phuong Ha Hoang, Minh Thi Nguyen: investigation; formal analysis; writing – original draft. Ke Son Phan, Huong Giang Bui, Anh Tuyet Thi Le: methodology; writing – review & editing. Thi Thu Huong Le, Nhat Huy Chu, Thu Trang Thi Mai, Dieu Thuy Thi Ung: conceptualization; methodology, writing – review & editing. Phuong Ha Hoang, Phuong Thu Ha: conceptualization; writing – review & editing; funding acquisition; supervision.

Conflicts of interest

There are no conflicts to declare.

Acknowledgements

This work financially supported by The National Office of Intellectual Property of Vietnam (Grant No. SHTT.TW 07-2022) to Phuong Ha Hoang. Minh Thi Nguyen was funded by Vingroup JSC and supported by the Master, PhD Scholarship Programme of Vingroup Innovation Foundation (VINIF), Institute of Big Data, code VINIF.2023.TS067.

Notes and references

1 J. Wang, D. Luo and J. Liu, *J. World Aquacult. Soc.*, 2023, **54**, 1337–1353.
2 E. S. Okeke, K. I. Chukwudozie, R. Nyaruaba, R. E. Ita, A. Oladipo, O. Ejeromedoghene, E. O. Atakpa, C. V. Agu and C. O. Okoye, *Environ. Sci. Pollut. Res. Int.*, 2022, **29**, 69241.
3 B. Suyamud, Y. Chen, D. T. T. Quyen, Z. Dong, C. Zhao and J. Hu, *Sci. Total Environ.*, 2024, **907**, 167942.
4 S. Zheng, Y. Wang, C. Chen, X. Zhou, Y. Liu, J. Yang, Q. Geng, G. Chen, Y. Ding and F. Yang, *Int. J. Environ. Res. Publ. Health*, 2022, **19**, 10919.
5 M. F. Warsito, *IOP Conf. Ser. Earth Environ. Sci.*, 2022, **1017**, 012026.
6 N. Nasrollahi, V. Vatanpour and A. Khataee, *Sci. Total Environ.*, 2022, **838**, 156010.

© 2025 The Author(s). Published by the Royal Society of Chemistry

Open Access Article. Published on 02 June 2025. Downloaded on 5/21/2026 6:09:23 AM. This article is licensed under a Creative Commons Attribution-NonCommercial 3.0 Unported Licence.

7 P. P. Singh, G. Pandey, Y. Murti, J. Gairola, S. Mahajan, H. Kandhari, S. Tivari and V. Srivastava, *RSC Adv.*, 2024, **14**, 20492–20515.
8 M. Fasnacht and N. Polacek, *Front. Mol. Biosci.*, 2021, **8**, 671037.
9 S. Thakur, A. Ojha, S. K. Kansal, N. K. Gupta, H. C. Swart, J. Cho, A. Kuznetsov, S. Sun and J. Prakash, *Adv. Powder Mater.*, 2024, **3**, 100233.
10 X. Liu, J. Pan, H. Huang, X. Zhang, N. Sun, C. Gu, Y. Zhuang and L. Wang, *Chem. Eng. J.*, 2023, **476**, 146868.
11 P. H. Hoang, M. T. Nguyen, K. S. Phan, H. G. Bui, T. T. H. Le, N. H. Chu, N. A. Ho, Q. H. Pham, X. K. Tran and P. T. Ha, *RSC Adv.*, 2024, **14**, 1984–1994.
12 C. J. Aul, M. W. Crofton, J. D. Mertens and E. L. Petersen, *Proc. Combust. Inst.*, 2011, **33**, 709–716.
13 N. Soni, N. Soni, R. Maheshwari, S. Thakkar, D. Sharma, R. K. Tekade, N. Sreeharsha and M. Tekade, *The Future of Pharmaceutical Product Development and Research*, 2020, pp. 413–446.
14 Y. Luo, Z. Liu, M. Ye, Y. Zhou, R. Su, S. Huang, Y. Chen and X. Dai, *Water*, 2024, **16**, 2586.
15 T. Sano, T. Ishii, K. Hotta and Y. Mano, *ACS Omega*, 2023, **8**, 36261–36268.
16 N. Zainol, K. A. Samad, C. A. Ilyana Che Jazlan and N. A. Razahazizi, *Heliyon*, 2022, **8**, e09217.
17 T. M. LaPara, J. E. Alleman, P. G. Pope, T. M. LaPara, J. E. Alleman and P. G. Pope, *Waste Manag.*, 2000, **20**, 295–298.
18 T. Kaur, A. Sraw, R. K. Wanchoo and A. P. Toor, *Sol. Energy*, 2018, **162**, 45–56.
19 A. H. Navidpour, B. Xu, M. B. Ahmed and J. L. Zhou, *Mater. Sci. Semicond. Process.*, 2024, **179**, 108518.
20 S. Karuppuchamy, K. Nonomura, T. Yoshida, T. Sugiura and H. Minoura, *Solid State Ionics*, 2002, **151**, 19–27.
21 P. S. M. Dunlop, T. A. McMurray, J. W. J. Hamilton and J. A. Byrne, *J. Photochem. Photobiol., A*, 2008, **196**, 113–119.
22 Y. Zhang, X. Zhao, S. Fu, X. Lv, Q. He, Y. Li, F. Ji and X. Xu, *Ceram. Int.*, 2022, **48**, 4897–4903.
23 E. V. Skorb, L. I. Antonouskaya, N. A. Belyasova, D. G. Shchukin, H. Möhwald and D. V. Sviridov, *Appl. Catal., B*, 2008, **84**, 94–99.
24 O. B. Ahmed and T. Alamro, *Sci. Rep.*, 2022, **12**, 18739.
25 V. K. Yemmireddy and Y. C. Hung, *Food Control*, 2017, **77**, 88–95.
26 J. Xie and Y. C. Hung, *Food Control*, 2019, **106**, 106690.
27 E. Jeong, H. Y. Park, J. Lee, H. E. Kim, C. Lee, E. J. Kim and S. W. Hong, *Environ. Res.*, 2021, **194**, 110657.
28 D. Venieri, I. Gounaki, M. Bikouvaraki, V. Binas, A. Zachopoulos, G. Kiriakidis and D. Mantzavinos, *J. Environ. Manage.*, 2017, **195**, 140–147.
29 U. Joost, K. Juganson, M. Visnapuu, M. Mortimer, A. Kahru, E. Nõmmiste, U. Joost, V. Kisand and A. Ivask, *J. Photochem. Photobiol., B*, 2015, **142**, 178–185.
30 M. Kook, H. Kaur, D. Danilian, M. Rosenberg, V. Kisand and A. Ivask, *J. Coat. Technol. Res.*, 2024, **21**, 1005–1016.
31 X. J. Yan, Y. Tang, C. Ma, Y. Liu and J. Xu, *Desalin. Water Treat.*, 2018, **124**, 160–176.
32 L. Cao, Z. Gao, S. L. Suib, T. N. Obee, S. O. Hay and J. D. Freihaut, *J. Catal.*, 2000, **196**, 253–261.
33 E. Jeong, H. Y. Park, J. Lee, H. E. Kim, C. Lee, E. J. Kim and S. W. Hong, *Environ. Res.*, 2021, **194**, 110657.
34 Y. Chen, H. Li, Z. Wang, T. Tao and C. Hu, *J. Environ. Sci.*, 2011, **23**, 1634–1639.
35 X. Sun, K. Xu, A. Chatzitakis and T. Norby, *J. Environ. Chem. Eng.*, 2021, **9**, 104809.
36 Y. Zhang, Q. Chen, H. Qin, J. Huang and Y. Yu, *Int. J. Environ. Res. Publ. Health*, 2022, **19**, 15550.
37 M. Raaja Rajeshwari, M. K. Okla, S. Kokilavani, M. A. Abdel-Maksoud, I. A. Saleh, H. A. Abu-Harirah, T. N. AlRamadneh and S. S. Khan, *Chemosphere*, 2023, **339**, 139529.
38 M. Motiei, L. Pleno de Gouveia, T. Sopík, R. Vícha, D. Skoda, J. Císař, R. Khalili, E. Domincová Bergerová, L. Münster, H. Fei, V. Sedlařík and P. Sáha, *Molecules*, 2021, **26**, 2067.
39 T. Liu, L. Wang, C. Sun, X. Liu, R. Miao and Y. Lv, *Chem. Eng. J.*, 2019, **358**, 1296–1304.
40 A. Gürses, M. Açıkyıldız, K. Güneş and M. S. Gürses, Dyes and pigments: their structure and properties, in *Dyes and Pigments*, Springer, Cham, 2016, pp. 13–29.
41 Y. Dai, M. Liu, J. Li, S. Yang, Y. Sun, Q. Sun, W. Wang, L. Lu, K. Zhang, J. Xu, W. Zheng, Z. Hu, Y. Yang, Y. Gao and Z. Liu, *Sep. Sci. Technol.*, 2020, **55**, 1005–1021.
42 J. Zambrano, P. A. García-Encina, J. J. Jiménez, R. López-Serna and R. Irusta-Mata, *J. Water Proc. Eng.*, 2022, **48**, 102841.
43 I. Aranaz, A. R. Alcántara, M. C. Civera, C. Arias, B. Elorza, A. H. Caballero, N. Acosta, H. Velasco, D. Mecerreyes, R. Antonio, B. Gimeno, A. María Díez-Pascual, V. C. Moreno and A. Serra, *Polymers*, 2021, **13**, 3256.
44 Y. C. Wang, H. Y. Lin and P. S. Chang, *Aquac Rep.*, 2023, **30**, 101615.
45 J. P. White and C. R. Cantor, *J. Mol. Biol.*, 1971, **58**, 397–400.
46 F. Yuan, C. Hu, X. Hu, D. Wei, Y. Chen and J. Qu, *J. Hazard. Mater.*, 2011, **185**, 1256–1263.
47 G. H. Lu, Y. H. Zhao, S. G. Yang and X. J. Cheng, *Bull. Environ. Contam. Toxicol.*, 2002, **69**, 111–116.
48 C. Munien, E. Kweinor Tetteh, T. Govender, S. Jairajh, L. L. Mguni and S. Rathilal, *Appl. Sci.*, 2023, **13**, 4766.
49 S. Heydari Orojlou, S. Rastegarzadeh and B. Zargar, *Sci. Rep.*, 2022, (12), 1–15.
50 D. Zhang, S. Lv and Z. Luo, *RSC Adv.*, 2020, **10**, 1275–1280.

© 2025 The Author(s). Published by the Royal Society of Chemistry